Discovering the feasibility of using the radiation forces for recovering rare earth elements from coal power plant by-products

Tran X. Phuoc*, Ping Wang, and Dustin McIntyre
National Energy Technology Laboratory,
Department of Energy, P. O. Box 10940, MS 84-340
Pittsburgh, PA 15261
* Corresponding author: tran@netl.doe.gov

Abstract

The feasibility of using laser separation for rare earth recovery from coal ashes was explored. To do so, laser-induced motion and travel distances of some rare earth and rare earth oxides (Lu_2O_3, Yb_2O_3, HfO_2, Dy_2O_3, Ta_2O_5, Tm, Lu, Ho, TeO_2, La_2O_3, Ho, TiO_2, Fe_2O_3 Y_2O_3, GeO_2, Sc_2O_3) and mineral compounds (MgO, CaO, Al_2O_3, SiO_2, KCl) that are commonly found is coal ashes were numerically investigated. The investigations were carried out for particles in quiescent air, (T = 300 K, $\mu = 18.46 \times 10^{-6}$ N-s/m^2 , $\rho = 1.177$ kg/m^3) exposing to a CW laser beam of 6 mm in diameter and it was focused by a 500 mm focal length lens. The results showed that the separation distances between these elements varied from few micrometers to several millimeters and it became widened as the laser power increased. The important result presented here is that all rare earth oxides were separated and concentrated in a small area located near the beam waist while all other mineral compounds traveled further and concentrated in a small area far from the beam waist.

Keywords: Photon pressure force, photophoretic force, rare earth element, coal ashes

Introduction

Recently, it has been reported that the concentrations of many rare earth elements in coal ashes could be enriched up to within the range of mineral ore deposits, suggesting that coal ashes are the potential resources for rare earth recovery [1, 2]. Several extraction methods have been used [2]. Generally, these procedures include initial acid leaching of ash materials, followed by material removal, separation, and purification. These separation steps are chemically intense and generate significant amount of waste streams because they require the use of large amount of water, leaching acids, caustic precipitates and organic solvents [3-6]. Each of these chemical components must be strictly handled to avoid unintended environmental release. The waste streams must be treated because coal ash residuals contain many trace elements that are hazardous elements with As, Cd, Hg, Pb, Se, and many others. For these reasons, there is a need for a safer, more environmental friendlier approach for rare earth recovery [7-17].

Sine a photon carries both energy and momentum, when it interacts with a particle, photon-particle energy and momentum transfer occurs resulting in mechanical forces acting on the particle. If the particle is absorptive, the energy transfer is significant, the particle is heated and a temperature

gradient exists on its surface. In this case, the force is categorized as the photophoretic force due to the surrounding gas molecules that rebound off the particle surface at different velocities. If the particle is non-absorptive or hardly absorbs the photon, the momentum transfer during refraction and reflection of the photon becomes dominant. In this case, the resulting force is called the photon pressure force. The pressure force composes of two forces: the gradient force acts transversely and the scattering (axial) force acts in the direction along with the photon propagation. Thus, when a laser beam is irradiated onto a coal ash cloud, the various elements of the coal ash will experience these radiation forces. They will be pulled into the higher intensity region of the beam in the transverse plane by the gradient force and simultaneously pushed along with the beam propagation direction by the scattering force. Since the magnitudes and directions of the radiation forces depend mainly on the particle properties such size, shape, thermal properties, and refractive index, these elements will move and displace at different speeds, directions, and distances, leading to spatial separations. This suggests that, by utilizing the radiation forces, the various components contained in a coal ash can be spatially separated and recovered without the need of using extraction solvents and leaching acids.

Use of a laser beam to manipulate and separate micron/nano-size particles has been reported [18-25]. In these studies, separation of transparent particles such as glass, silica, PMMA, polystyrene, nickel and aluminum oxides particles in water using a loosely focused Gaussian beam were investigated. The effects of various parameters including, numerical aperture, focal length, laser power, particle size, refractive index, and medium velocity on the parting distance, the number particles separated per unit time were studied. This study will explore the feasibility of using the radiation forces for sorting and separating the various rare earth compounds contained in coal fly and bottom ashes. It is noted that laser separation of particles is achieved based on the motion and displacement, known as the retention distance of each particle induced by the thermal/momentum exchange between particles and photons carried by the laser beam. To explore such feasibility we, therefore, will conduct a series of numerical calculations given to the laser-induced motion of some typical rare earth compounds that are commonly found to present in coal ashes. The goal is to evaluate and observe the differences in their trajectories, their retention distances as they move down stream and finally escape from the laser beam. The calculations will be carried using quiescent air as a medium. Separation of rare earth compounds from coal ash in air is more preferable in terms of environmental impact. Other advantages are due the low viscosity and refractive index of air. A low refractive index leads to a greater radiation force. Thus, particles in air will move faster and farther resulting in a larger separation distance and higher separation throughput. In addition, since these compounds may include both absorptive and non-absorptive species, the photon force equations developed by the previous investigators might not be useful. We, therefore, will develop a system of equations that accounts for the result of the particle extinction coefficient for this proposed application.

Theoretical Consideration

When a particle is dropped into a loosely focused laser beam, since the curvature of the wave is negligible [18, 26], photon streams are assumed to travel in the direction parallel to the laser propagation direction and interact with the particle via reflection, refraction, absorption, and transmission as represented in Fig.1. The forces acting on the particle are: the gravity force, the photophoretic force, the photon pressure force, and the viscous force. The gravity force, F_g induces the particle downwards motion. The photophoretic force F_{phtr}, which is due to the particle heating, controls the axial motion of the particle. The photon pressure force, which is induced by the direct transfer of the photon momentum to the particle during refraction and reflection, composes of two components: the scattering component F_x controlling the particle axial motion and the gradient component, F_y controlling the particle motion in the direction perpendicular to the axial direction. The viscous force, which is resulted due to the particle motion, resists the particle motion. Therefore, the particle motion in x and y-directions can be described as

$$\rho_p \frac{4\pi a^3}{3} \frac{dv_x}{dt} = F_x + F_{phtr} - F_{d,x} \tag{1}$$

$$\rho_p \frac{4\pi a^3}{3} \frac{dv_y}{dx} = F_y - F_{d,y} - F_g \tag{2}$$

The x-component velocity, v_x and the y-component velocity, v_y are

$$\frac{dx}{dt} = v_x \tag{3}$$

$$\frac{dy}{dt} = v_y \tag{4}$$

In these equations, $F_g = 4\pi a^3 \rho_p g/3$ is the gravity force, ρ_p is the particle density, a is the particle radius, g is the gravitational accelerator. The drag forces $F_{d,x}$ and $F_{d,y}$ acting on the particle in x and y-directions, respectively, are

$$F_{d,x} = 6\pi a \mu v_x \tag{5}$$

$$F_{d,y} = 6\pi a \mu v_y \tag{6}$$

Where μ is the viscosity of the medium. It has been known that, in the limit where the Knudsen numbers Kn = l/a, (where l is the mean free path of the molecules of the surrounding gas and a is the particle size) are considerably less than 1 a surface temperature gradient can cause molecules of the surrounding gas slide over the particle surface from colder to hotter parts of the surface due to the phenomenon known as Maxwellian Creep. As a result, a tangential stress on the particle surface is created. If the surface temperature gradient is due to a non-uniform heating of the particle

by an optical field, this force is called photophoretic force [27-32]. Yalamov et al. [22] solved the boundary value problem for the spherical geometry and the force is given

$$F_{phtr} = -\frac{4\pi a K \mu^2 I_o K_a J_1}{\rho T k_p} \tag{7}$$

Where I_o is the laser intensity which is given as

$$I_o = \frac{2P_o}{\pi}\int_{-\pi/2}^{\pi/2}\frac{1}{w^2}\exp\left(-\frac{2r^2}{w^2}\right)\sin\theta d\theta \tag{8}$$

and K is the thermal slip factor (from 3/4 to 1.7), ρ is the medium density, T is the temperature of the medium surrounding the particle, k_p is the thermal conductivity of the particle, K_a is the absorption factor, and J_1 is the asymmetry factor which is the most important factor that determines the magnitude and the direction of the force. For particles with sizes such that $2\pi k_2 a/\lambda$ (where k_2 is the extinction coefficient, λ is the wave length) is small, the back side of the particle will be more heated than the front one, J_1 has a positive value indicating that the force pushes the particle toward the radiation source. As $2\pi k_2 a/\lambda$ increases, the back side of the particle will be heated less intensively than the front side one, J_1 becomes negative. In this case, the particle is pushed away from the radiation source. To calculate J_1 and K_a, the distribution of the elctromagnetic field within the particle must be known. Numerical calculations for J_1 were performed using the complete Mie formula for the internal field [27-31]. In the case where the particle is large, based on the Fresnel's formulas for amplitudes of reflected and refracted waves, Yalamov et al. [32] have reported an approximate analytical calculation for J_1 from ray optics as

$$J_1 = 3N_2 k_2 \xi \int_0^1 \frac{F_1 s}{\psi_1}\left\{-\left(1-s^2\right)^{1/2} + \frac{1}{\psi_1} - \left[\left(1-s^2\right)^{1/2} + 2\delta_1 + \frac{1}{\psi_1}\right]\exp\left(-2\psi_1\left[\left(1-s^2\right)^{1/2} + \delta_1\right]\right)\right\} ds \tag{9}$$

$$K_a = 4N_2 k_2 \xi \int_0^1 \frac{F_1 s}{\psi_1}\left\{1 - \exp\left(-2\psi_1\left[\left(1-s^2\right)^{1/2} + \delta_1\right]\right)\right\} ds \tag{10}$$

Where

$$F_1 = 2\left(1-s^2\right)\left\{\frac{1}{\left[\left(1-s^2\right)^{1/2} + \left(N_2^2 - s^2\right)^{1/2}\right]^2} + \frac{N_2^2}{\left[N_2^2\left(1-s^2\right)^{1/2} + \left(N_2^2 - s^2\right)^{1/2}\right]^2}\right\} \tag{11}$$

$$\psi_1 = 2N_2 k_2 \xi\left[\frac{1}{1 - \frac{s}{N_2}\left(N_2^2 - 1\right)\left(1-s^2\right)}\right]\frac{\left(1-s^2\right)^{1/2}}{\left(N_2^2 - s^2\right)^{1/2}} \tag{12}$$

$$\delta_1 = \frac{s^2}{N_2^2}\left[\left(N_2^2 - s^2\right)^{1/2} - \left(1 - s^2\right)^{1/2}\right] \tag{13}$$

Where $\xi = 2\pi a/\lambda$ is the size parameter, N_2 is the particle refractive index, and k_2 is the particle extinction coefficient. Typical results for J_1 and K_a calculated from Eqns (9) and (10) are shown in Fig. 2. For the particle size up to 18 μm, increasing the particle extinction coefficient k_2 results in a significant increase in the absorption factor K_a while for the asymmetry factor J_1, increasing k_2 leads to not only a significant increase in its magnitude but also a change in its direction. For example, for $k_2 = 0.001$, J_1 was always positive and increased to a value of about 0.03. For $k_2 = 0.01$, J_1 increased positively initially then became negative after the particle size increased larger than 3 μm. For $k_2 = 0.1$, however, it had negative values for the entire range of the particle size used here. The results shown here also indicate that for a highly absorptive particle, J_1 and K_a can reach a limiting value of - 0.5 and 1, respectively. In this case one can assume that the particle behaves as the blackbody and absorbs the laser beam entirely at its illuminated surface. Since the asymmetry factor indicates the direction of the photophoretic force, the results shown here indicate that both the magnitude and the direction of the photophoretic force depend significantly on the particle size and its extinction coefficient. Regardless of the particle size, hardly absorptive particles (for example $k_2 \leq 0.001$) will experience a negative photophoretic force that acts against the propagation direction of the radiation beam pulling them upstream toward the radiation source while highly absorptive particles (for example $k_2 \geq 0.1$) will experience a positive photophoretic force that pushes them away from the radiation source. For particles with extinction coefficients somewhere in between, however, the direction of the photophoretic force is changing depending on the particle size, it acts as a pulling force for small particles and becomes a pushing force for larger particles.

The photon pressure force is induced by the direct photon-particle momentum interaction during refraction and reflection. When the particle size is much larger than the laser wavelength the photon pressure force can be determined by ray optics [26, 33, 34]. These available models were developed mainly for non-absorbing particles ($k_2 = 0$). This study explores the use of these radiation forces for separation of particles which involve with both absorbing and non-absorbing particles. In this case, the force equations that can account for the effect of the particle extinction coefficient, k_2 must be used. Thus, following the derivation given by Phuoc [35] the x and y components for the force equations are

$$F_x = \frac{2N_1 P_o a^2}{c_o}\int_{-\pi/2}^{\pi/2}\frac{1}{w^2}\exp\left(-\frac{2r^2}{w^2}\right)\left(1 - R\cos\beta_R + H_x\right)\sin\theta d\theta \tag{14}$$

$$H_x = \sum_1^N (-1)^I R^{I-1}(1-R)^2 \exp\left(-\frac{2\pi I k_2 \delta}{\lambda}\right)\cos\beta_T \tag{15}$$

$$F_y = -\frac{2N_1 P_o a^2}{c_o}\int_{-\pi/2}^{\pi/2}\frac{2}{w^2}\exp\left(-\frac{2r^2}{w^2}\right)\left(R\sin\beta_R - H_y\right)\sin\theta d\theta \tag{16}$$

$$H_y = \sum_1^N (-1)^I R^{I-1}(1-R)^2 \exp\left(-\frac{2\pi l k_2 \delta}{\lambda}\right)\sin\beta_T \tag{17}$$

Where

$$\theta_1 = \theta \tag{18}$$

$$N_1 \sin\theta_1 = N_2 \sin\theta_2 \tag{19}$$

$$\delta = 2a\cos\theta_2 \tag{20}$$

$$\beta_R = \pi - 2\theta_1 \tag{21}$$

$$\beta_{T_n} = 2n\theta_1 - 2\theta; \quad n = 1, 3, 5,... \tag{22a}$$

$$\beta_{T_n} = \pi + 2n\theta_1 - 2\theta; \quad n = 2, 4, 6,... \tag{22b}$$

The Fresnel reflectance R is given by

$$R = \frac{1}{2}\left[\frac{\sin^2(\theta_1 - \theta_2)}{\sin^2(\theta_1 + \theta_2)} + \frac{\tan^2(\theta_1 - \theta_2)}{\tan^2(\theta_1 + \theta_2)}\right] \tag{23}$$

Where c_o is the speed of light in vacuum, N_1 is the refractive index of the medium, P_o is the total power, r is the radial distance from the beam's axis, w is the beam width and it is calculated as a function of the beam waist w_o, beam diameter d, and lens' focal length as

$$w = w_o + 2x\left(\frac{d - w_o}{2f}\right) \tag{24}$$

If the focal region of the beam is assumed to be cylindrical in shape, the focal spot size, in terms of the beam waist w_o is given as

$$w_o = \frac{2\lambda}{\pi}\frac{f}{d} \tag{25}$$

If the particle is at a distance h from the beam center, the radial distance r is approximated as

$$r = \left(h^2 + a^2\sin^2\theta + 2ha\sin\theta\right)^{1/2} \tag{26}$$

Numerical Calculation Results

We present in Fig.3 the typical considered results for the two constituents of the radiation pressure force acting on a particle located at different locations across the laser beam for two locations along the beam propagation axis: $x = 0$ is the location at the beam waist, $x > 0$ is the location away from the beam waist. Since the extinction coefficient k_2 is set equal to zero, the photophoretic force does not exist and it is not included in this figure. It is clear that, the magnitudes of the scattering force F_x and the gradient force F_y acting on the particle located across the laser beam were always symmetrical around the beam center and they decreased significantly in the course of the beam propagation. The scattering force was always positive while the gradient force was negative when the particle was in the upper half of the laser beam and it became positive when the particle was in the lower half of the beam [36-39]. Therefore, the gradient force is the only component of the radiation pressure that tends to push the particle toward the beam center. For a horizontally propagating beam, such as the case presented here, this is the only force component that acts in the direction with the gravity force when the particle is in the upper half and against the gravity force when the particle is in the lower half. Thus, if it is greater than the gravity force, the particle will remain in the laser beam for being transported along the beam propagation direction by the scattering component. For example, the typical results presented here indicate that F_y was greater than the gravity force F_g at the beam waist, $x = 0$. Thus, the particle will remain within the laser beam and travel along the laser beam. Since the beam width expands in the propagation course, the magnitudes of both F_y and F_x decrease and F_y might become less than F_g as typically shown in Fig. 3 at $x = 1.5$ mm. In this case, the particle will fall out of the laser beam.

To investigate the effects of the particle refractive index, N_2, on the radiation pressure, we show in Fig. 4 the gradient and the scattering forces across the beam waist for three different values of N_2 while keeping $N_1 = 1$ and $k_2 = 0$. As it is shown, when N_2 increased, the direction of the forces did not alter. The magnitude of the scattering force, however, increased significantly while that of the gradient force decreased moderately. As described by Eqns. (1) to (4), when a particle is dropped into a laser beam, its motion is induced by the scattering force, gradient force, the gravity force, and the drag force. Its axial travel distance, therefore, depends on whether it can be retained within the laser beam or not. As the particle is in the upper half of the laser beam, the gradient force is negative. Thus, while moving in the laser propagation direction due to the scattering force, it is also moving downwards due to the gravity force and the gradient force. As the particle passes the beam centerline into the lower half, the gradient force becomes positive acting against the gravity force. Thus, if the magnitude of the gradient force is less than that of the gravity force, the downwards motion continues and the particle will drop out of the laser beam. On the other hand, if the magnitude of the gradient force is greater than that of the gravity force, the downwards motion is reversed. In this case, the particle is pushed up and retains vertically in the laser beam and continues moving along with the direction of the laser propagation. Since both the gradient force and the axial force decrease as the particle moving with the laser beam, the particle will regain the downwards motion and eventually drops out of the laser beam when the gradient force

has decreased to lower than the gravity force. Since the gradient force is the principal force that acts against the gravity force in order to retain the particle within the laser beam, the decrease in the gradient force with increasing N_2, although it is moderate as shown in Fig. 4, will have a significant impact on laser particle transport and separation. To demonstrate the impact of the particle refractive index on the particle motion, we show in Fig. 5 the trajectories of a 10 μm particle. The results show that the particle with $N_2 = 4$ continuously moved downwards and dropped out of the beam after traveling with a distance of about 609 μm. This is because the gradient force acting on this particle was not strong enough to act against the gravity force in order to retain the particle in the laser beam. For the particle with $N_2 = 1.5$, since the gradient force acting on it was strong enough to act against the gravity force, the reversal of the downwards motion was seen to occur at x = 129 μm, the particle moved upwards then regained its downwards motion again at x = 294 μm. Although the axial force acting on this particle was the least, it was able to travel with a longest distance of about 1.12 mm.

Effects of the extinction coefficient k_2 on the gradient force F_y, the scattering force F_x, and the photophoretic force F_{phtr} are shown in Figs 6 and 7. The results showed that an increase in k_2 leads to an increase in the magnitudes of F_x and F_{phtr} but a decrease in magnitude of F_y. The pronounced effect observed here, however, is the change in the direction of both the gradient force F_y and the photophoretic force F_{phtr}. For example, the photophoretic force F_{phtr} was negative with $k_2 = 0.001$ and it became positive and increased significantly for $k_2 \geq 0.01$. For values of k_2 less than 0.01, the gradient force was attractive with negative values on the particle located in the upper half and positive values on the particles located in the lower half. In this case, the force will pull the particle toward the beam center. For $k_2 = 0.1$, it became repulsive with positive values acting on the particle located in the upper half and negative values on the particle in the lower half. In this case, the force will push the particle away from the laser beam. Thus, comparing with a transparent or less absorptive particle, a highly absorptive particle might possibly travel with a shorter distance because it can be pushed out of the laser beam before it is effectively pushed downstream by the photophoretic and the axial forces [40-45].

To explore the feasibility of using the photophoresis forces presented above for separating the various elements contained in a coal ash, we carried out a series of calculations on the trajectories of some rare earth and rare earth oxides and mineral compounds that are commonly found in coal ashes. These elements are chosen because their thermal and optical properties are available for our present calculations. The calculations were carried out for particles in quiescent air, (T = 300 K, $\mu = 18.46 \times 10^{-6}$ N-s/m^2 , $\rho = 1.177$ kg/m^3) exposing to a laser beam of 6 mm in diameter and it is focused by a 500 mm focal length lens. The results are tabulated in Table 1. The trajectories of some rare earth oxides are also presented in Fig. 8 for easy reference.

It is clear that all elements travelled with different travel distances which varied from about 100 μm to about 4 mm. The shortest travel distances were obtained for Lu_2O_3 and Yb_2O_3 while SiO_2 and KCl were among the elements that traveled with the longest distances. The separation distances between these elements varied from few micrometers to several millimeters and it

became widened as the laser power increased. The differences in the travel distances reported here are due to the differences in the element optical properties, density, and thermal conductivity. For transparent elements ($k_2 = 0$), although element density has some affects, the effect of the refractive index was seen to be significant because it has a significant effect on the gradient force as shown in Fig. 4. For example, the travel distance obtained for TiO_2 with $N_2 = 2.82$ was 1.643 mm for $P_o = 1.5$ W and 3.080 mm for $P_o = 3$ W. For the same laser powers, GeO_2, with $N_2 = 1.612$, was able to travel with longer distances, (2.349 mm for $P_o = 1.5$ W and and 4.112 mm for $P_o = 3$ W) although it is much heavier than TiO_2 (density of GeO_2 is 4250 kg/m^3 and the density of TiO_2 are 3970 kg/m^3). For absorptive elements ($k_2 \neq 0$), the effect of the extinction coefficient k_2 seemed to be more important. For example, although the density of Ta_2O_5 is much less than that of HfO_2 the separation distance between these elements was only 19 μm apart. This is because the extinction coefficient k_2 of Ta_2O_5 is too small and the photophoretic force acting on it was negative resisting its motion.

The important result presented here is that Ho, Lu, Tm and other rare earth oxides were seen to concentrate in the upstream region while all mineral oxides concentrated in the downstream region of the laser beam. These two regions were separated by about 300 μm for $P_o = 1.5$ W and 500 μm for $P_o = 3$ W. As far as separation of rare earth elements from coal ashes is concerned, this result is significant. Since laser parameters such as beam shape, beam diameter, focal length, etc… also have significant effects on the separation distance, a laser separation system can be designed such that these two areas can be distinguishably far apart. The materials in each area, therefore, are collected separately for further processing and purification.

Conclusions

We have conducted a numerical study to explore the feasibility of laser separation for recovery of rare earth elements from coal ashes. The calculations were performed for some rare earth oxides and mineral oxides that are commonly found in coal ashes. The results indicate that, under laser action, these oxide particles were moving along with the laser propagation direction and finally dropped out of the laser beam into two small areas that were several millimeters apart. The rare earth oxides were seen to concentrate in the area near the beam waist while the mineral oxides mainly concentrated in the area further away from the beam waist. This suggests a new potential separation method that rare earth elements in coal ashes can be separated and recovered without the need of using leaching acids and other toxic separation solvents. The present study, however, is preliminary. Similar results were previously reported by others [16, 46-48]. Continuing studies which investigate into the effect of the various laser parameters such as beam shape, beam diameter and focal length on the separation throughput together with experimental observations are being conducted. The results will be reported in due course.

Table. 1 Travel distances from the beam waist showing that Ho, Lu, Tm and other rare earth oxides concentrated in the upstream region while all mineral oxides concentrated in the downstream region. These two regions are separated by about 300 μm for $P_o = 1.5$ W and 500 μm for $P_o = 3$ W. ($N_1 = 1$, $\lambda = 532$ nm, beam diameter = 6 mm, focal length = 500 mm, particle radius = 5 μm Particle in still air at 300 K, $\mu = 18.46 \times 10^{-6}$ N-s/m^2 , $\rho = 1.177$ kg/m^3)

Elements	n	k	ρ (kg/m^3)	k_p (W/m.K)	Travel Distance (mm)	
					$P_o = 1.5$ W	3.0 W
Lu_2O_3 (Lutetium oxide)	1.943	0.0	9420	--------	0.096	0.195
Yb_2O_3 (Ytterbium oxide)	1.956	0.0	9170	--------	0.099	0.254
HfO_2 (Hafnium foxide)	2.120	0.0	9680	--------	0.103	0.187
Dy_2O_3 (Dysprosium Oxide)	1.9865	0.0	7810	--------	0.121	2.451
Ta_2O_5 (Tantalum pentoxide)	2.163	0.000033	8200	0.2-0.35	0.128	2.228
Tm (Thulium)	1.978	2.4767	9330	16.9	1.033	2.718
Lu (Lutetium)	1.855	3.17	9840	16.00	1.102	2.767
TeO_2 (Tellurium dioxide)	2.300	0.0	5670	3.0	1.498	2.898
La_2O_3 (Lanthanum oxide)	1.88	0.0	6510	--------	1.501	2.915
TiO_2 (Titanium oxide)	2.82	0.0	3970	--------	1.643	3.080
Ho (Holmium)	1.5485	1.9708	8330	16.00	1.665	3.683
Fe_2O_3 (Iron oxide)	1.986	0.0	5240	--------	1.829	3.367
Y_2O_3 (Yttrium oxide)	1.94	0.0	5010	27.0	1.935	3.517
GeO_2(Germanium oxide)	1.612	0.0	4250	--------	2.349	4.112
Sc_2O_3 (Scandium oxide)	2.003	0.0	3860	--------	2.413	4.193
MgO (Magnesium oxide)	1.73	0.0	3540	--------	2.735	4.657
CaO (Calcium oxide)	1.83	0.0	3300	--------	2.860	4.831
Al_2O_3 (Alumina)	1.773	0.0	3000	--------	3.116	5.193
SiO_2 (Silicon dioxide)	1.46	0.0	2170	--------	3.959	6.388
KCl (potassium chloride)	1.493	0.0	1980	--------	4.261	6.814
Sc (Scandium)	1.0734	1.1498	2840	15.80	4.674	7.259

recommendation, or favoring by the United States Government or any agency thereof. The views and opinions of authors expressed herein do not necessarily state or reflect those of the United States Government or any agency thereof."

References

1. V.V Seredin and S. Dai, Coal Deposits a potential alternative sources for lanthanides and yttrium, *International Journal of Coal Geology*, **94**, 67-93 (2012).
2. D.B.Mayfield, and A.S Lewis, Enviromental review of coal ash as a resource for rare earth and strategic elements, 2013 World of Coal Ash (WOCA) Conference, April 22-25, 2013, Lexington, KY (http://www.flyash.info].
3. J.C. Hower, D. Shifeng, V. V. Serendin, Z. Lixin, I.J Kostova, L.F.O. Silva, S. Mardon, A Note on the Occurrence of Yttrium and Rare Earth Elements in Coal Combustion Products, *Coal Combustion and Gasification Products*, **5**, 39-47 (2013).
4. J. Ribeiro, S.R. Taffarel, C.H. Sampaio, D. Flores, L.F.O. Silva, Mineral speciation and fate of some hazardous contaminants in coal waste pile from anthracite mining in Portugal, *International Journal of Coal Geology*, **109-110**, 15-23 (2013a).
5. J. Ribeiro, K. DaBoit, D. Flores, M.A. Kronbauer, L.F.O. Silva, Extensive FE-SEM/EDS, HR-TEM/EDS and ToF-SIMS studies of micron- to nano-particles in anthracite fly ash, *Science of the Total Environment*, **452-453**, 98-107 (2013b).
6. L.F.O. Silva, S. Fdez-Ortiz de Vallejuelo, I. Martinez-Arkarazo, K. Castro, M.L.S. Oliveira, C.H. Sampaio, I.A.S de Brum, F.B. De Leão, S.R. Taffarel, J.M Madariaga, Study of environmental pollution and mineralogical characterization of sediment rivers from Brazilian coal mining acid drainage, *Science of the Total Environment*, **447**, 169-178 (2013)
7. M.L.S. Oliveira, C.R. Ward, C.H. Sampaio, X. Querol, C.M.N.L. Cutruneo, S.R. Taffarel, L.F.O. Silva, Partitioning of Mineralogical and Inorganic Geochemical Components of Coals from Santa Catarina, Brazil, by Industrial Beneficiation Processes, *International Journal of Coal Geology*, **116**, 75-92 (2013).
8. M.L.S. Oliveira, C.R Ward, D. French, J.C. Hower, X. Querol, L.F.O. Silva, Mineralogy and leaching characteristics of beneficiated coal products from Santa Catarina, Brazil, *International Journal of Coal Geology*, **94**, 314-325 (2012a).
9. M.L.S. Oliveira, C.R. Ward, M. Izquierdo, C.H. Sampaio, I.A.S. de Brum, R.M. Kautzmann, S. Sabedot, X. Querol, L.F.O. Silva, L.F.O, Chemical composition and minerals in pyrite ash of an abandoned sulphuric acid production plant, *Science of the Total Environment*, **430,** 34-47 (2012b).
10. D. Quispe, R. Pérez-López, L.F.O. Silva, J.M. Nieto, Changes in mobility of hazardous elements during coal combustion in Santa Catarina power plant (Brazil), *Fuel*, **94**, 495-503 (2012).
11. L.F.O. Silva, J.C. Hower, M. Izquierdo, X. Querol, Complex nanominerals and ultrafine particles assemblages in phosphogypsum of the fertilizer industry and implications on human exposure, *Science of the Total Environment*, **408**, 5117-5122 (2010).
12. L.F.O. Silva, M. Izquierdo, X. Querol, R.B. Finkelman, M.L.S. Oliveira, M. Wollenschlager, M. Towler, R. Pérez-López, F. Macias, Leaching of potential hazardous elements of coal cleaning rejects. *Environmental Monitoring and Assessment*, **175**, 109-126 (2011a).

13. L.F.O. Silva, M. Wollenschlager, M.L.S. Oliveira, A preliminary study of coal mining drainage and environmental health in the Santa Catarina region, Brazil, *Environmental Geochemistry and Health,* **33**, 55-65 (2011b).
14. L.F.O. Silva, C.H. Sampaio, A. Guedes, S. Fdez-Ortiz de Vallejuelo, J.M. Madariaga, Multianalytical approaches to the characterisation of minerals associated with coals and the diagnosis of their potential risk by using combined instrumental microspectroscopic techniques and thermodynamic speciation, *Fuel*, **94,** 52-63 (2012).
15. C.M.N.L. Cutruneo, M.L.S. Oliveira, S.R. Ward, J.C. Hower, I.A.S. de Brum, C.H. Sampaio, R.M. Kautzmann, S.R. Taffarel, E.C. Teixeira, I.F.O. Silva, A mineralogical and geochemical study of three Brazilian coal cleaning rejects: Demonstration of electron beam applications. *International Journal of Coal Geology*, **130**, 33-52 (2014).
16. J. Ribeiro, K. DaBoit, D. Flores, C.R. Ward, L.F.O. Silva, Identification of nanominerals and nanoparticles in burning coal waste piles from Portugal, *Science of the Total Environment*, **408**, 6032-6041 (2010).
17. B.K. Saikia, C.R. Ward, M.L.S. Oliveira, J.C. Hower, M. Braga, L.F.O. Silva, Geochemistry and nano-mineralogy of two medium-sulfur Northeast Indian coals, *International Journal of Coal Geology*, **122**, 26-34 (2014).
18. S. Koyanaka and S. Endoh, The effect of relative refractive index on monosized particle movement under laser radiation pressure, *Advanced Powder Technology*, **10,** 205-222 (1999).
19. S. Koyanaka and S. Endoh , Numerical simulation of the optical system and medium flow field suitable for particle separation using laser radiation pressure, *Advanced Powder Technology*, **15,** 321-336 (2004).
20. S. Koyanaka and S. Endoh , Effect of laser scanning on increase of throughput in particle separation using laser radiation pressure, *Advanced Powder Technology*, **15,** 337-349 (2004)
21. B.S. Zhao, Y.M. Koo, D.S. Chung, Separations based on the mechanical forces of light, *Analytica Chimica Acta* **556**, 97–103 (2006)
22. S. Koyanaka and S. Endoh, Three-dimensional analysis of the movement of various micron-sized particles under laser radiation pressure, *Powder Technology* **116**, 13–22 (2013)
23. A.A. Lall, A. Terray, and S. J. Hart, On-the-fly cross flow laser guided separation of aerosol particles based on size, refractive index and density–theoretical analysis, *Optics Express*, **18,** 26775-26790 (2010)
24. M. Zabetian, M. S. Saidi, M. B. Shafii, and M. H. Saidi, Separation of microparticles suspended in a minichannel using laser radiation pressure, *Applied Optics*, **52**, 4950-4958 (2013).
25. H. Xin, D. Bao, F. Zhong, B. Li, Photophoretic separation of particles using two tapered optical fibers, *Laser Phys. Lett*. **10**, 036004 (8pp) (2013).
26. S. B. Kim and S.S. Kim, Radiation forces on spheres in loosely focused Gausian beam: ray optics regime, *J. Opt. Soc. Am*. **B 23**, 897-903 (2006).
27. D.W. Mackowski, Photophoresis of aerosol particles in the free molecular and slip-flow regimes, *Int. J. Heat. Mass Transfer*, **32**, 843-854 (1989).

28. W.M. Greene, R.E. Spjut, E. Ba-ziv, J.P. Longwell, and A.F. Sarofim, Photophoresis of irradiated spheres: Evaluation of the complex Index of refraction, *Langmuir* **1**, 361-365 (1985).
29. W.M. Greene, R.E. Spjut, E. Ba-ziv, A.F. Sarofim, and J.P. Longwell, Photophoresis of irradiated spheres: Absorption centers, *J. Opt. Soc. Am*., **B 2**, 998-1004 (1985).
30. A.B. Pluchio, Photophoretic force on particles for low Knudsen number, *Applied Optics*, **22**, 103-106 (1983).
31. S.A. Beresnev, and L.B. Kochneva, Radiation aborption asymmetry factor and photophoresis of aerosols, *Institute of Atmospheric Optics*, **16**, 119-126 (2003).
32. Y.I. Yalamov, V.B Kutukov, and E.R. Shchukin, Theory of the photophoretic motion of the large-size volatile aerosol particle, *Journal of Colloid and Interface Science*, **57**, 564-571 (1976).
33. S. Nemoto, H. Togo, Axial force acting on a dielectric sphere in a focused laser beam, *Appl. Opt*. **37**, 6386-6394 (1998).
34. R.C. Gauthier, S. Wallace, Optical levitation of pheres: Analytical development and numerical computations of the force equations, *J. Opt. Soc. Am*. **12**, 1680-1686 (1995).
35. T.X. Phuoc, A numerical study of the radiation forces on an absorbing particle using the ray optics approach, *Optics Communications*, **241**, 271–277 (2004).
36. D. Arenas-Lago, F.A. Veja, L.F.O. Silva, M.L. Andrade, Soil interaction and fractionation of added cadmium in some Galician soils, *Microchemical Journal*, **110**, 681-690 (2013).
37. B. Cerqueira, F.A. Vega, L.F.O. Silva, M.L. Andrade, Effects of vegetation on chemical and mineralogical characteristics of soils developed on a decantation bank from a copper mine, *Science of the Total Environment*, **421-422,** 220-229 (2012).
38. B. Cerqueira, F.A.Vega, C. Serra, L.F.O. Silva, M.L. Andrade, Time of flight secondary ion mass spectrometry and high-resolution transmission electron microscopy/energy dispersive spectroscopy: A preliminary study of the distribution of Cu2+ and Cu2+/Pb2+ on a Bt horizon surfaces, *Journal of Hazardous Materials*, **195**, 422-431 (2011).
39. J.C. Hower, J.M.K. O'Keefe, K.R. Henke, N.J. Wagner, G. Copley, D.R. Blake, T. Garrison, M.L.S. Oliveira, R.M. Kautzmann, L.F.O. Silva, Gaseous emissions and sublimates from the Truman Shepherd coal fire, Floyd County, Kentucky: A re-investigation following attempted mitigation of the fire, *International Journal of Coal Geology*, **116**, 63-74 (2013)
40. K. O. Garcia, E.C Teixeira, D.M Agudelo-Castaneda, M. Braga, P.G. Alabarse, F. Wiegand, R.M. Kautzmann, L.F.O. Silva, Assessment of nitro-polycyclic aromatic hydrocarbons in PM1 near an area of heavy-duty traffic. *Science of the Total Environment*, **479-480**, 57-65 (2014).
41. C.L. Dias, M.L.S. Oliveira, J.C. Hower, S.R. Taffarel, R.M. Kautzmann, L.F.O. Silva, Nanominerals and ultrafine particles from coal fires from Santa Catarina, South Brazil, *International Journal of Coal Geology*, **122**, 50-60 (2014).

42. M.A. Kronbauer, M. Izquierdo, S. Dai, F.B. Waanders, N.J. Wagner, M. Mastalerz, J.C. Hower, M.L.S. Oliveira, S.R. Taffarel, D. Bizani, L.F.O. Silva, Geochemistry of ultra-fine and nano-compounds in coal gasification ashes: A synoptic view, *Science of the Total Environment*, **456-457**, 95-103 (2013).
43. K. Martinello, M.L.S. Oliveira, F.A. Molossi, C.G. Ramos, E.C. Teixeira, R.M. Kautzmann, L.F.O. Silva, Direct identification of hazardous elements in ultra-fine and nanominerals from coal fly ash produced during diesel co-firing, *Science of the Total Environment*, **470-471**, 444-452 (2014).
44. F. Pérez, M. Llorca, M. Kock-Schulmeyer, B. Krbi, M.L.S. Oliveira, K. Da Boit Martinello, N.A. Al-Dhabi, I. Anti, M. Farré, D. Barcelò, Assessment of perfluoroalkyl substances in food items at global scale, *Environmental Research*, **135**, 181-189 (2014).
45. N. Rodríguez-Vázquez, S. Salzinger, L.F.O.Silva, M. Amorín, J.R. Granja, Synthesis of Cyclic γ-Amino Acids for Foldamers and Peptide Nanotubes, *European Journal of Organic Chemistry*, **2013**, 3477-3493 (2013)
46. L.F.O. Silva, X. Querol, K.M. da Boit, S. Fdez-Ortiz de Vallejuelo, J.M. Madariaga, Brazilian Coal Mining Residues and Sulphide Oxidation by Fenton s Reaction: an accelerated weathering procedure to evaluate possible environmental impact, *Journal of Hazardous Materials* **186**, 516-525 (2011a).
47. L.F.O. Silva, F. Macias, M.L.S. Oliveira, M.K. da Boit, F. Waanders, Coal cleaning residues and Fe-minerals implications. *Environmental Monitoring and Assessment*, **172**, 367-378 (2011b)
48. L.F.O. Silva, M.L.S. Oliveira, R.N. Erika, J.M.K. OKeefe, K.R. Henke, J.C. Hower, Nanominerals and ultrafine particles in sublimates from the Ruth Mullins coal fire, Perry County, Eastern Kentucky, USA, *International Journal of Coal Geology*, **85**, 237-245 (2011c).

List of Figures

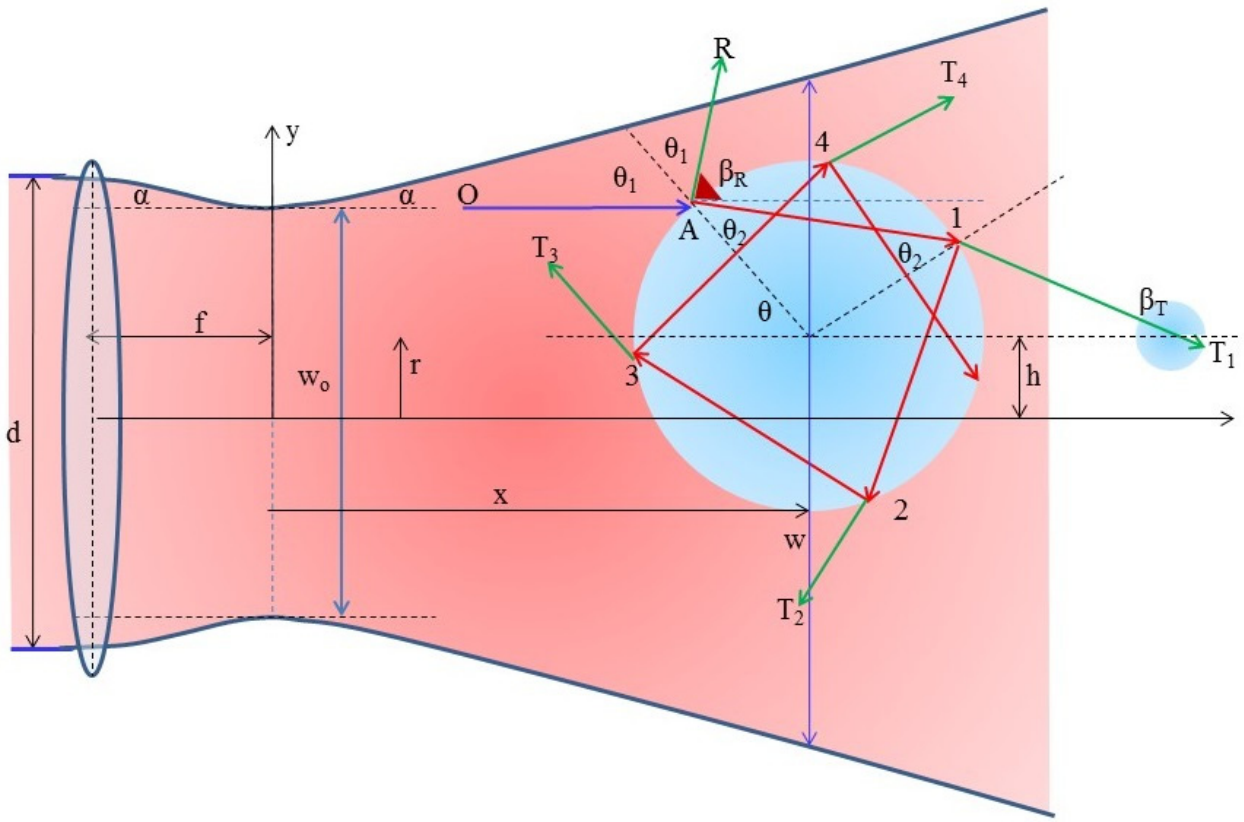

Figure 1. Geometrical representation of a Gaussian beam and its interaction with a particle showing the photon ray OA, its reflection AR and refraction at A1 and multiple internal reflection beams: 12, 23, 34, etc. and multiple transmission beams $1T_1$, $2T_2$, $3T_3$, $4T_4$, etc. (d is the beam diameter, f is the focal length, w_o is the beam waist, w is the beam width, r is the beam radius h is the distance from the particle to the beam center, x is the location of the particle in the x-direction, y is the vertical directionα is the beam divergent angle, β_R is the reflection angle of AR, β_T is the angle makes by the transmission beam with x-direction, and θ, θ_1, and θ_2 are angles as indicated in the figure) (correction made as suggested by reviewer 4)

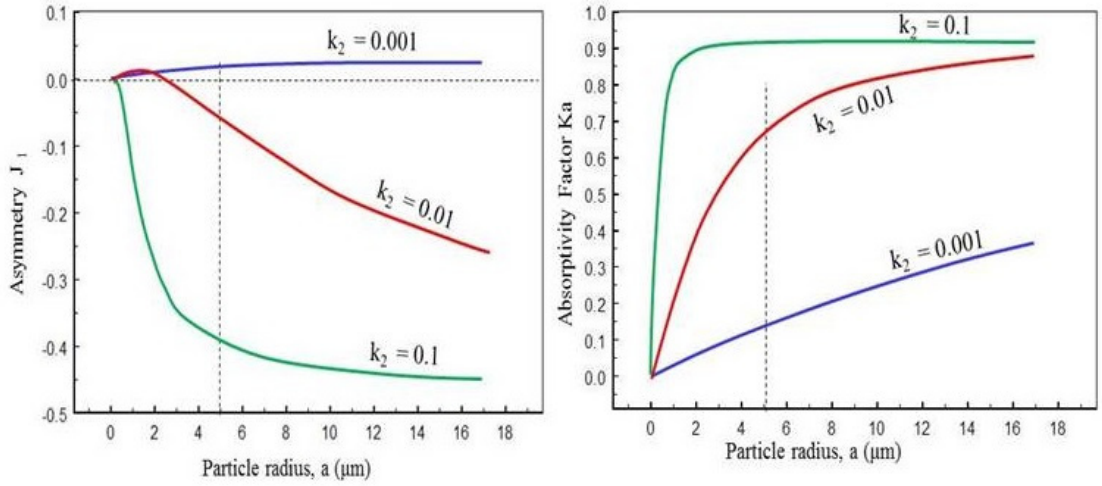

Figure 2. Asymmetry factor J_1 and absorption factor K_a

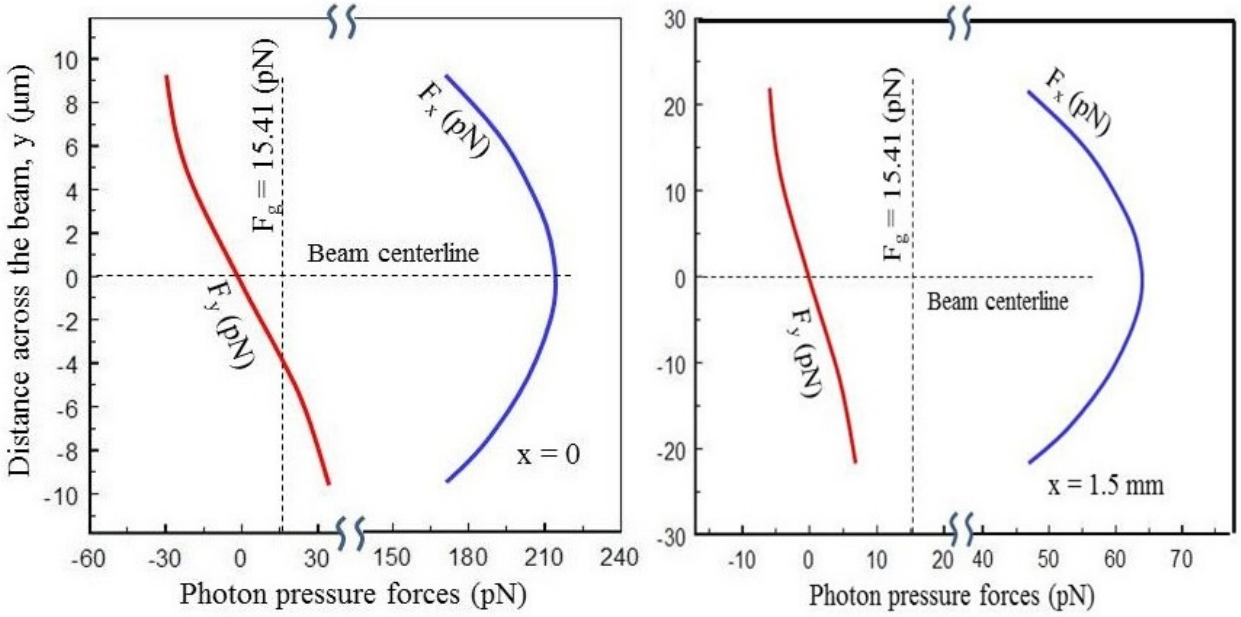

Figure 3. The scattering and the gradient components of the photon pressure acting on a particle (N_1 = 1, N_2 = 1.5, k_2 = 0.0, ρ_p = 3000 kg/m^3 , λ = 532 nm, P_o = 1.5 W, beam diameter d = 6 mm, focal length f = 500 mm, particle radius = 5 μm)

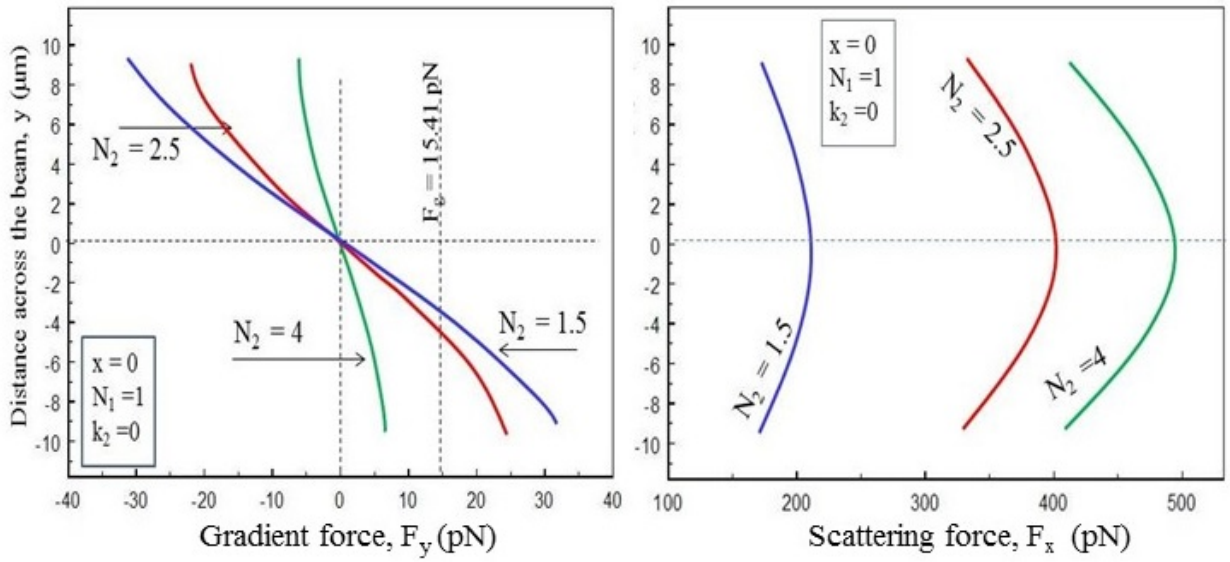

Figure 4. Effect of the refractive index N_2 on the scattering and the gradient components of the photon pressure acting on a particle ($N_1 = 1$, $k_2 = 0$, $\rho_p = 3000$ kg/m^3 , $\lambda = 532$ nm, $P_o = 1.5$ W, beam diameter = 6 mm, focal length = 500 mm, particle radius = 5 μm)

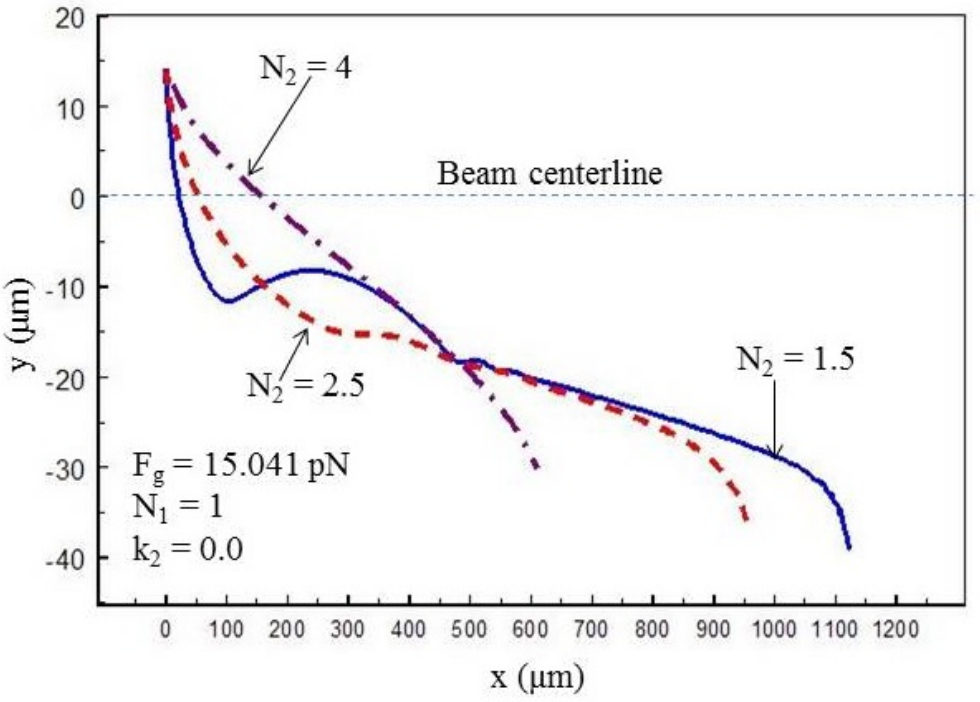

Figure 5. The effect of N_2 on the trajectory of the particle the following conditions ($N_1 = 1$, $k_2 = 0.0$, $\rho_p = 3000$ kg/m^3 , $\lambda = 532$ nm, $P_o = 1.5$ W, beam = 6 mm, focal length f = 500 mm particle radius a = 5 μm, Particle in still air at 300 K, $\mu = 18.46 \times 10^{-6}$ N-s/m^2 , $\rho = 1.177$ kg/m^3 . The gravity force was calculated to be 15.41 pN.

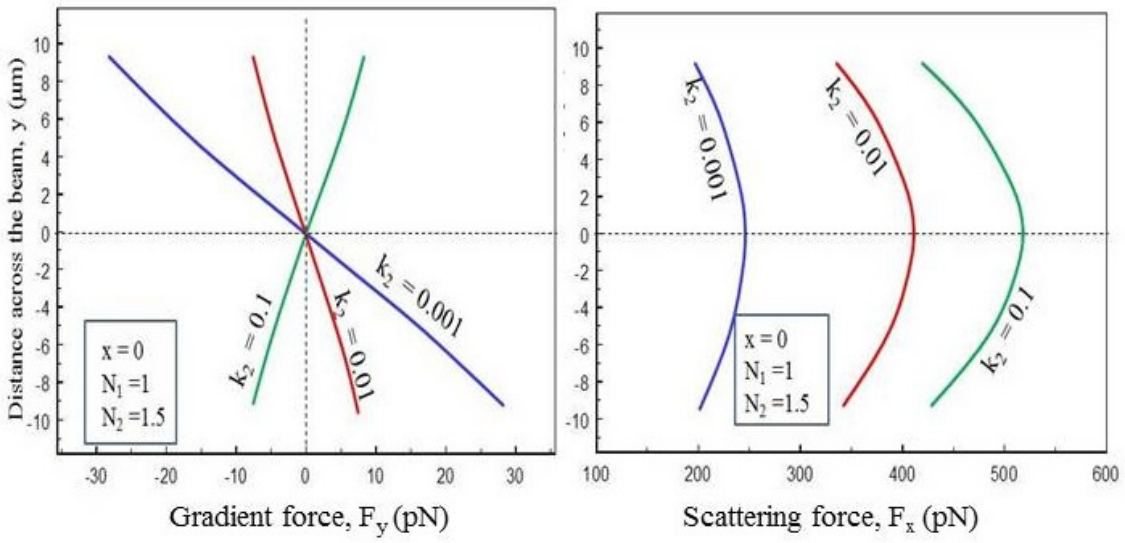

Figure 6. Effect of the extinction coefficient k_2 on the scattering and the gradient components of the photon pressure acting on a particle ($N_1 = 1$, $N_2 = 1.5$, $\rho_p = 3000$ kg/m^3 , $\lambda = 532$ nm, $P_o = 1.5$ W, beam diameter 6 mm, focal length f = 500 mm, particle radius = 5 μm)

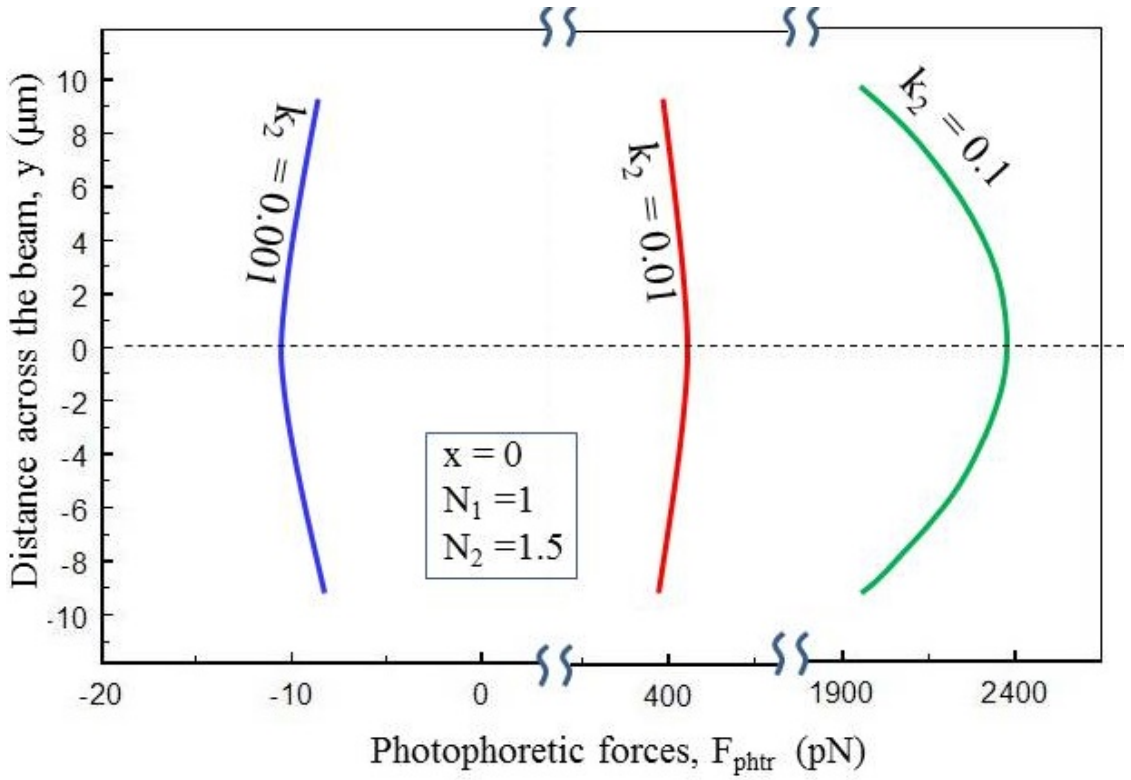

Figure 7. Effect of the extinction coefficient k_2 on the photophoretic force acting on a particle (N_1 = 1, N_2 = 1.5, ρ_p = 3000 kg/m^3 , λ = 532 nm, P_o = 1.5 W, beam diameter 6 mm, focal length 500 mm, thermal conductivity λ_p = 12 W/m-K, particle radius = 5 μm)

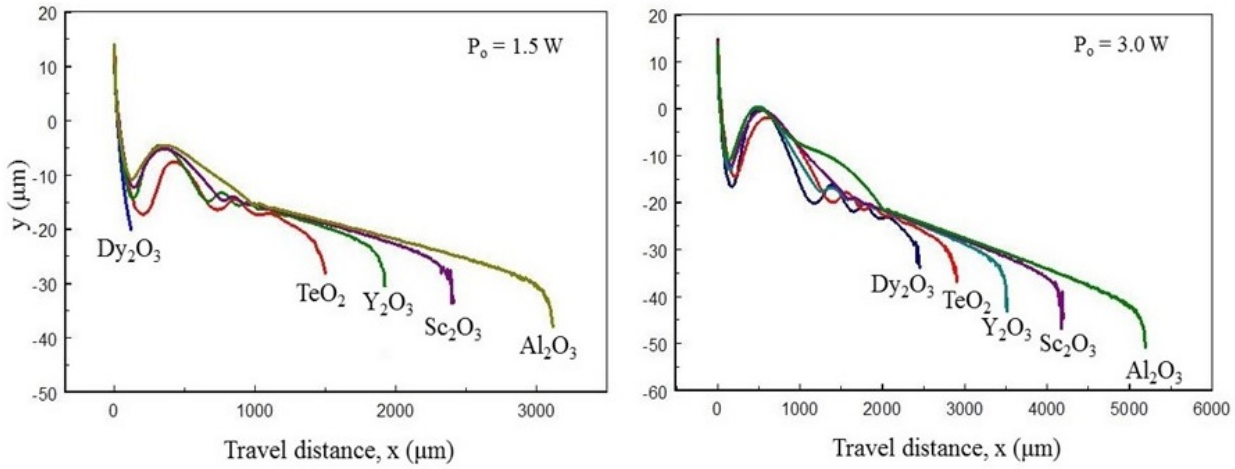

Figure 8. Travel distances for some elements (N_1 = 1, λ = 532 nm, beam = 6 mm, focal length f = 500 mm particle radius a = 5 μm, Particle in still air at 300 K, μ = 18.46 x 10^{-6} N-s/m^2, ρ = 1.177 kg/m^3)